

Proximity Driven Enhanced Magnetic Order at Ferromagnetic Insulator / Magnetic Topological Insulator Interface

Mingda Li,^{1,2,3,*} Cui-Zu Chang,^{2,†} B. J. Kirby,⁴ Michelle Jamer,⁵ Wenping Cui,⁶ Lijun Wu,³ Peng Wei,² Ferhat Katmis,² Yimei Zhu,³ Don Heiman,⁵ Ju Li,^{1,7} and Jagadeesh S. Moodera^{2,8,‡}

¹*Department of Nuclear Science and Engineering,*

Massachusetts Institute of Technology, Cambridge, MA 02139, USA

²*Francis Bitter Magnet Lab, Massachusetts Institute of Technology, Cambridge, MA 02139, USA*

³*Condensed Matter Physics and Materials Science Department,*

Brookhaven National Laboratory, Upton, New York 11973, USA

⁴*Center for Neutron Research, National Institute of Standards and Technology, Gaithersburg, Maryland 20899, USA*

⁵*Department of Physics, Northeastern University, Boston, MA 02115, USA*

⁶*Department of Physics, Boston College, Chestnut Hill, MA 02467, USA*

⁷*Department of Material Science and Engineering,*

Massachusetts Institute of Technology, Cambridge, MA 02139, USA

⁸*Department of Physics, Massachusetts Institute of Technology, Cambridge, MA 02139, USA*

(Dated: April 8, 2015)

Magnetic exchange driven proximity effect at a magnetic insulator / topological insulator (MI/TI) interface provides a rich playground for unexpected phenomena as well as a way to realize low energy dissipation quantum devices. Here we report a tripled enhancement of proximity exchange coupling in the MI/magnetic-TI EuS / $\text{Sb}_{2-x}\text{V}_x\text{Te}_3$ hybrid heterostructure, where V doping is used to drive the TI (Sb_2Te_3) to be magnetic. We observe an artificial antiferromagnetic-like structure created between the two strong ferromagnets, which may account for the enhancement of interfacial proximity coupling. The interplay between the proximity effect and doping in hybrid heterostructure provides insights into the engineering of magnetic ordering.

PACS numbers: 61.05.fj, 75.25.-j, 75.30.Gw, 75.70.Cn.

The time-reversal symmetry (TRS) breaking and surface bandgap opening of topological insulator (TI) is an essential step towards the observation of novel quantum phases and realization for TI-based devices [1, 2]. In general, there are two approaches to break the TRS: transitional metal (TM) ion doping, where Cr or V are doped into the entire TI [3, 4], and magnetic proximity effect, where a magnetic insulator (MI) layer in proximity to TI induces exchange coupling [3, 5–7]. Doping TM impurities into TI will introduce a perpendicular ferromagnetic (FM) anisotropy and provide a straightforward means to open up the bandgap of the TI's surface state, with profound influence to its electronic structure [4, 8–13]. In particular, quantum anomalous Hall effect (QAHE), where quantum Hall plateau and dissipationless chiral edge channels emerge at zero external magnetic field, has recently been realized in Cr-doped and V-doped TIs [8, 9, 14–19]. Ideally, compared to the doping method, the proximity effect has a number of advantages, including spatially uniform magnetization, better controllability of surface state, freedom from dopant-induced scattering that degrades TI properties, as well as preserving TI intrinsic crystalline structure, etc. [20, 21]. However, due to the in-plane anisotropy and low Curie temperature of the common MI, such proximity effect is usually too weak to induce strong proximity magnetism in TI. In fact, compared to magnetically doped TI which could induce as large as a 50 meV surface bandgap [4], the EuS/TI system has only 7 meV gap opening due to

the strongly localized Eu-f orbitals [22]. Therefore, the enhancement of proximity magnetism is highly desirable to make it a valuable approach as doping hence takes full advantage.

In this *Letter*, we report significant enhancement of the proximity effect in MI EuS / magnetic-TI $\text{Sb}_{2-x}\text{V}_x\text{Te}_3$ hybrid heterostructure. Using polarized neutron reflectometry (PNR), we observe an increase of proximity magnetization per unit cell (u.c.) in TI, from $1.3\mu_B/\text{u.c}$ to $3.4\mu_B/\text{u.c}$ at $x = 0.1$ doping level. The great advantage is that Eu's has a large magnetic moment ($\sim 7.9\mu_B/\text{ion}$) as well as one of the largest thermal neutron absorption in the periodic table ($\sigma_A(\text{Eu}) = 4530\text{b}$, 10^3 times greater than the other elements in the system of interest). This helps in identifying the EuS interface sharpness and excludes interdiffusion of Eu ions into the TI without ambiguity, as employed recently [21]. Furthermore, the proximity effect enhancement is accompanied by a decrease in the interfacial magnetization of EuS, resulting in an exotic antiferromagnetic (AF) like structure. The existence of the “artificial” AF structure between FM EuS and the FM $\text{Sb}_{2-x}\text{V}_x\text{Te}_3$ with different anisotropies is confirmed by exchange bias measurements. Such AF ordering is not natural and commonly expected between two FMs. The hybrid heterostructure shows unexpected features, for engineering and designing of novel magnetic structures.

High-quality MI 6 nm EuS / 15 quintuple (QL) magnetic TI $\text{Sb}_{2-x}\text{V}_x\text{Te}_3$ hybrid heterostructures were grown

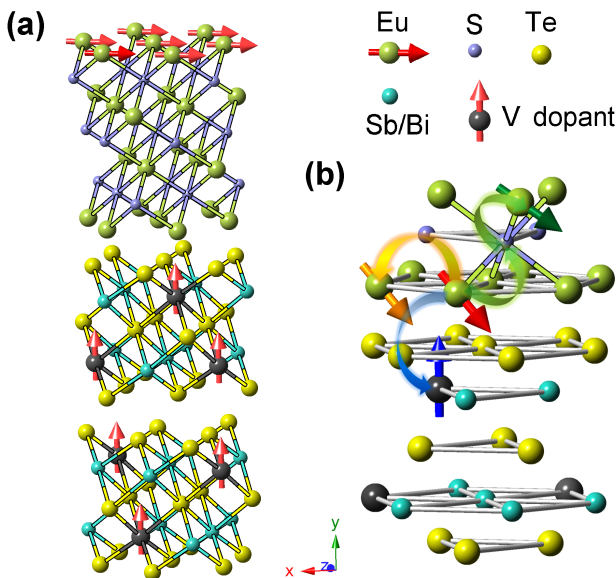


FIG. 1. (color). (a) MI EuS / V-doped TI Sb_2Te_3 hybrid heterostructure. The arrows denote the spin direction. The V-doped TI layer has a perpendicular magnetic anisotropy, while the magnetic EuS has in-plane magnetic anisotropy. Such heterostructure may create an exotic magnetic environment near the interface, as illustrated in (b). For a given Eu ion (red-arrow), it interacts with neighborhood intra-plane Eu (orange arrow) through Heisenberg interaction, inter-plane Eu ions (green arrow) through super-exchange interaction, spin-polarized states at TI surface and localized moments in TI (blue arrow).

by molecular beam epitaxy (MBE) under a base vacuum $\sim 5 \times 10^{-10}$ Torr, where magnetic TI thin films $\text{Sb}_{2-x}\text{V}_x\text{Te}_3$ were grown on clean, heat-treated sapphire (0001) substrates with V-dopants coevaporated during TI growth. The EuS (111) layer was deposited *in situ* over the TI film using electron beam source. To understand the interplay between proximity effect and TM doping, 6 nm EuS/ 15 QL Sb_2Te_3 , 15 QL $\text{Sb}_{2-x}\text{V}_x\text{Te}_3$ and 15 QL $\text{Sb}_{2-x}\text{V}_x\text{Te}_3$ samples were fabricated.

The atomic configuration of the MI / magnetic TI heterostructure is shown in Fig. 1 (a). The upper EuS has in-plane anisotropy [23–26] within xz -plane, while the lower TM doped TI has easy axis out-of-plane [9, 13, 19] along y -axis. The different anisotropy directions in the two layers, corroborated by a strong interfacial spin-orbit coupling, create a complex magnetic environment for the EuS near the interface (Fig. 1 b). The Heisenberg interaction, superexchange interaction [24, 27], $d-f$ coupling [28] and coupling with the TI's spin texture may finally contribute to an overall augmentation of the proximity effect.

The PNR experiments were carried out at NG-D Reflectometer at the NIST Center for Neutron Research, from which the in-plane component of magnetization can be extracted. The experimental setup is shown in Fig.

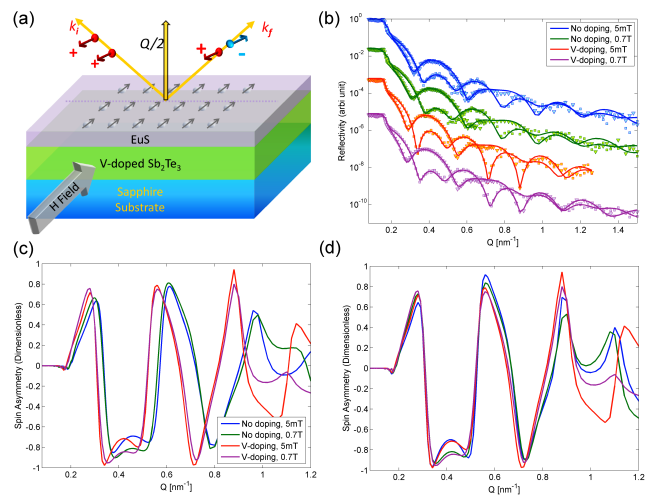


FIG. 2. (color). (a) The configuration of specular PNR. k_i , k_f and Q denote the incident wavevector, reflected wavevector and the momentum transfer, respectively. (b) The spin + and spin - PNR data R^+ and R^- for the EuS/ $\text{Sb}_{1.9}\text{V}_{0.1}\text{Te}_3$ and EuS/ Sb_2Te_3 samples, at low (5 mT) and high (0.7 T) in-plane guiding fields. The fitting results are represented by solid lines and the curves are shifted for clarity. (c) The spin asymmetry for the reflectivity in b. (d) The same spin asymmetry, but assuming one control sample EuS/ Sb_2Te_3 have exactly the same thickness as EuS/ $\text{Sb}_{1.9}\text{V}_{0.1}\text{Te}_3$. In this way, the spin asymmetry difference is dominated by only the magnetic structure instead of crystalline structure. At $\sim 0.4 \text{ nm}^{-1}$, the difference comes from the effect of external magnetic field, while at $\sim 1.0 \text{ nm}^{-1}$ the difference mainly comes from V-dopants.

2(a), where the incident spin-polarized neutron beam is reflected by the heterostructure sample, while the spin non-flip reflectivity signals from both spin components ($++$ and $--$) were collected under external guiding magnetic field.

The spin non-flip reflectivity curves for the MI/ magnetic TI sample EuS/ $\text{Sb}_{1.9}\text{V}_{0.1}\text{Te}_3$ and control sample MI/TI EuS/ Sb_2Te_3 , at low (5 mT) and high (0.7 T) fields, are shown in Fig. 2 (b). The fitting and refinement of PNR is performed using the GenX program [29]. To directly infer the possible contribution of V-dopants, the corresponding spin asymmetries $SA = \frac{R^+ - R^-}{R^+ + R^-}$ are plotted (Fig. 2c) for the raw data and thickness-adjusted data (Fig. 2d). In this way, the different features of the SA in Fig. 2 (d) are solely coming from the magnetic structure since the crystalline structure is taken to be identical. We see that at $Q \sim 0.4 \text{ nm}^{-1}$, $H = 5 \text{ mT}$ SA for both samples with and without V-dopants overlap each other, but distinct with the $H = 700 \text{ mT}$ SA curves, indicating an effect from guiding field within this Q range; while at $Q \sim 1.0 \text{ nm}^{-1}$, a splitting of the SA curves for both samples at same guiding field (eg. blue and red curves) is observed. This indicates the influence of the V-dopants to magnetic structure at high Q range (spatially localized) even without performing fitting.

Results of fitting the PNR data are shown in Fig. 3. The substrate lies in the region below 0 nm. Nuclear- SLD (NSLD, red curves) identifies the chemical compositional contrast, where the NSLDs for each compound layer are correctly reproduced from PNR fitting (sapphire substrate $5.5 \times 10^{-5} \text{ nm}^{-2}$, Sb_2Te_3 $1.8 \times 10^{-4} \text{ nm}^{-2}$, EuS $1.5 \times 10^{-4} \text{ nm}^{-2}$ and amorphous Al_2O_3 capping layer $4 \times 10^{-4} \text{ nm}^{-2}$). This further validates the fitting quality. In Fig. 3(a), without the EuS proximity layer, the V-dopants in the $\text{Sb}_{1.9}\text{V}_{0.1}\text{Te}_3$ sample contribute to no more than $0.2\mu_B/\text{u.c}$ in-plane magnetization at $H = 0.7 \text{ T}$, indicating a very strong perpendicular FM anisotropy in V-doped TI. This is consistent with the result in the inset of Fig. 4 (a), and facilitates us in obtaining reliable PNR refinement by fixing the magnetization of the magnetic TI layer. The magnetic- SLD (MSLD) (blue curves) at $H = 5 \text{ mT}$ and 700 mT in-plane guiding fields at $T = 5 \text{ K}$ are also plotted. In Fig. 3 (b), for the EuS /pure TI sample, we see a penetration of magnetization into TI. Unlike the EuS region where strong absorption LSD (ASLD) is always accompanied due to the Eu ions' large neutron absorption, the magnetization into TI does not show any absorption ($\sim 14\text{--}15 \text{ nm}$), indicating that such magnetism in TI is not from ferromagnetic Eu ions interdiffused into Sb_2Te_3 , but from proximity exchange effect. The free of interdiffusion is also consistent with our Transmission Electron Microscopy (TEM) result in Fig. 3(d), where a sharp interface between epitaxially grown EuS and $\text{Sb}_{1.9}\text{V}_{0.1}\text{Te}_3$ is developed.

The magnetization at the interface in proximity structures is greatly enhanced when V-dopant is at present, from $1.3\mu_B/\text{u.c}$ (Fig. 3b, without V-doping) to $3.4\mu_B/\text{u.c}$ (Fig. 3c, V-doped), i.e. almost tripled. In both cases, the penetration depth of proximity is $\sim 1 \text{ nm}$, consistent with $\text{Bi}_2\text{Se}_3 / \text{EuS}$ interface [21]. Besides, the in-plane magnetization of EuS drops dramatically near the interface, from $\sim 3\mu_B/\text{u.c}$ without V-dopants to $\sim 0.5\mu_B/\text{u.c}$ with V-doping, at $H = 5 \text{ mT}$. This is due purely to magnetic effect instead of interfacial roughness since the ASLD is flat near the TI interface. On the contrary, magnetization drop at $\text{EuS} / \text{Al}_2\text{O}_3$ interface ($\sim 23 \text{ nm}$) is due to the Stranski-Krastanov growth [30], leading to a thickness variation and formation of island. This is directly confirmed from Z-contrast high-angle angular dark field (HAADF) TEM image (Fig. 3(d)). At higher field $H = 0.7 \text{ T}$, an increase of the in-plane EuS magnetism is accompanied with a drop of proximity effect into TI. Since only the perpendicular direction magnetism will contribute to the proximity effect [1], a high in-plane guiding field tends to align the EuS moment in-plane and reduce the proximity.

To understand the origin of the in-plane EuS magnetism drop near the interface, we performed magnetic hysteresis measurements using superconducting quantum interference device (SQUID) in a Physical Property Measurement System (PPMS). We use Bi_2Te_3 instead

of Sb_2Te_3 since Both belong to Bi_2Se_3 TI family and share very similar crystalline structure. Despite Sb_2Te_3 is more suitable for PNR studies due to less interstitial V-defects, Bi_2Te_3 is more suitable for SQUID due to higher diamagnetic susceptibility. We adopt the traditional approach for exchange bias (EB) measurement [31–33] at various reset fields by applying $H = -1 \text{ T}$ saturation field each time before the measurement to prevent EB training effect [34]. The results for coercivity $H_c \equiv (H_{c2} - H_{c1})/2$ and bias field $H_{bias} \equiv (H_{c2} + H_{c1})/2$ are plotted in Fig. 4(d). Although H_c remains constant, a reset-field-dependent H_{bias} is observed including a sign change. This strongly suggests an existence of AF structure and a likely magnetic frustration [35], and is quite striking since our system is only composed by two strong FMs.

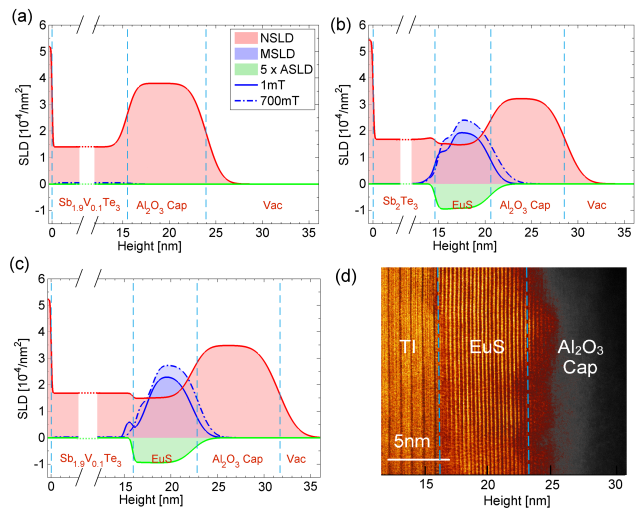


FIG. 3. (color). PNR fitting profiles of doping-only sample $\text{Sb}_{1.9}\text{V}_{0.1}\text{Te}_3$ (a), proximity only sample $\text{EuS} / \text{Sb}_2\text{Te}_3$ (b) and hybrid heterostructure sample $\text{EuS} / \text{Sb}_{1.9}\text{V}_{0.1}\text{Te}_3$ (c). The NSLD, MSLD and ASLD denote the nuclear, magnetic and absorption scattering length density, respectively. The proximity effect appears as finite magnetization signal (blue curves) in the region of TI near the interface ($\sim 15 \text{ nm}$). The absorption free feature in this region excludes the possible contribution of interdiffused Eu ions. We see clearly that with V-doping, the proximity magnetism is enhanced as a bump in (c), accompanied with a further suppression of magnetism of interfacial EuS ($15\text{--}18 \text{ nm}$). (d) HAADF TEM image of the $\text{EuS} / \text{Sb}_{1.9}\text{V}_{0.1}\text{Te}_3$ hybrid heterostructure. A sharp interface between the TI / MI is developed, indicating an epitaxial growth of EuS , consistent with (c) for uniformly distributed ASLD of EuS . The island-like crystalline facets between EuS and Al_2O_3 cap explains the roughness in (c).

To further understand the implication of the results in Fig. 4, we develop a phenomenological energy model to describe the coupling between the FM and AF. The anisotropic energy for bulk EuS can be written as [25]

$$E_{an} = \kappa_1 M_s t (\alpha_1^2 \alpha_2^2 + \alpha_1^2 \alpha_3^2 + \alpha_3^2 \alpha_2^2) + \kappa_2 M_s t \alpha_1^2 \alpha_2^2 \alpha_3^2 \quad (1)$$

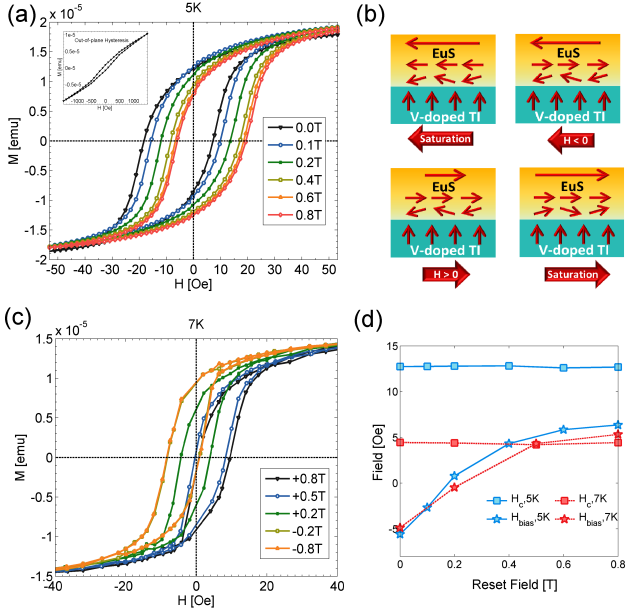


FIG. 4. (color). The in-plane magnetic hysteresis of 2nm EuS / 10 QL Bi_{0.1}V_{0.1}Te₃ hybrid heterostructure, at 5 K (a) and 7 K (c). A clear EB has been observed by switching to different reset fields. To prevent exchange bias training effect, a -1 T saturation field is applied before each measurement. Inset is the out-of-plane magnetic hysteresis of the same sample, where the magnetism is quite hard and hysteresis loop closes above ~ 2 T. The possible configuration derived from EB in (d) is shown in (b), where V-doped TI is kept perpendicular anisotropy, but an interfacial AF structure is created to cause the EB.

where α_i is the directional cosine along i^{th} direction, M_s is the saturation magnetism per area, t is the thickness of FM layer and the anisotropic constants $\kappa_1 = -19.6$ Oe and $\kappa_2 = -4.6$ Oe at $T = 1.3$ K [25]. Since our interest is in thin film structures with a single symmetry axis (y -axis in Fig. 1 a), eq. (1) could be rewritten as using a simplified model for hexagonal and cubic lattice [36],

$$E_{an} = K_1 M_s t \sin^2(\theta) + K_2 M_s t \sin^4(\theta) \quad (2)$$

where $K_1 = \kappa_1 = -19.6$ Oe, $K_2 = -\frac{7}{8}\kappa_1 + \frac{1}{8}\kappa_2 = 16.6$ Oe, θ is the angle between the magnetization and the symmetry axis. Since $K_1 < 0$, $\theta = \pi/2$ corresponds in the present case for EuS showing easy-plane anisotropy within xz -plane. For a thin film, we further define $K_{1,eff} = K_s/t + K_1$. We require the surface anisotropy constant $K_s > 0$, since for thinner sample $K_{1,eff}$ will approach zero from the negative side, indicating a rotation of the in-plane easy plane to an out-of-plane direction, resulting in a magnetic canting which is reasonable for compensated thin film interfaces [32, 37].

Taking into account the external magnetic field H and the FM/AF coupling J , the total energy could be written

TABLE I. Temperature dependence of the anisotropy constants. Green, Blue, red and black colored values are from [25], eq. (5), measurements in Fig.4 and eq. (4), respectively.

$T_c = 17$ K	1.3 K	5 K	7 K
K_1 (Oe)	-19.6	-13.10	-9.96
K_2 (Oe)	+16.6	7.41	4.29
H_c (Oe)	N/A	12.7	4.4
K_s/t (Oe)	13.8	9.3	7.2; 7.1

as

$$E = -HM_s t \sin(\theta) - J \sin(\theta) + \left(K_1 + \frac{K_s}{t}\right) M_s t \sin^2(\theta) + K_2 M_s t \sin^4(\theta) \quad (3)$$

At saturation field configuration $\theta = \pm\pi/2$ and considering the energy extreme, we obtain the bias field and coercivity

$$H_{bias} = -\frac{J}{Mt}, \quad H_c = 2K_1 + 4K_2 + \frac{2K_s}{t} \quad (4)$$

respectively.

The anisotropic coefficients strongly depend on temperature [36]. In the mean-field approximation, the temperature dependence of anisotropy can be expressed using the Callen and Callen theory as [38, 39]

$$K(T) = K(0) \left(1 - \frac{T}{T_c}\right)^{\frac{n(n+1)}{4}} \quad (5)$$

where n is the order of anisotropy constant, $n(K_1) = 2$ and $n(K_2) = 4$. Assuming that the Curie temperature of EuS is $T_c = 17$ K, we obtain the temperature dependence of anisotropy constants as shown in Table I. One remarkable feature for this model is that the surface anisotropy K_s/t calculated from experimental values and eq. (4) coincides with the independent check using eq. (5), giving 7.2 Oe vs 7.1 Oe at 7 K. Finally, this yields a surface anisotropy $K_s = 0.0014$ erg \cdot cm $^{-2}$ by assuming a 2.5×10^{-5} emu saturation and 5 mm 2 sample area. This term is the origin of magnetic canting of interfacial EuS.

Contrary to the strong T -dependence of anisotropy, the bias field H_{bias} thus AF/FM coupling constant J has a weak dependence with temperature, indicating an origin of FM/AF coupling different from magnetic crystalline anisotropy such as the prominent role of Spin-Orbit interaction and spin-momentum locking at the surface of the TI.

To summarize, we have observed a large enhancement of proximity exchange coupling strength in MI/magnetic-TI hybrid heterostructure. This overcomes the major

disadvantage in MI/TI heterostructures where the proximity coupling strength is considered to be weak [22]. To our knowledge, this is also the first report unifying the two independent approaches to magnetize TIs utilizing both TM doping and proximity exchange coupling. Here, the magnetic dopants magnetize the surface states in TI, which are further coupled to the MI; whereas the magnetic TI has a strong perpendicular anisotropy that compensates the weakness of MI having in-plane anisotropy. We use a phenomenological energy model to obtain a $K_s = 0.0014 \text{ erg} \cdot \text{cm}^{-2}$ surface anisotropy. Despite this value being small compared to the stronger examples such as the Au/Co interface [40], this approach provides insights to tailor new magnetic structure at TI/MI interfaces.

M. L. would thank the helpful discussion with Prof. C.X. Liu. J.S.M. and C.Z.C would thank support from the STC Center for Integrated Quantum Materials under NSF grant DMR-1231319, NSF DMR grants 1207469 and ONR grant N00014-13-1-0301. M. J. and D. H. acknowledge support from NSF DMR-907007 and NSF ECCS-1402738.

* mingda@mit.edu

† czchang@mit.edu

‡ moodera@mit.edu

- [1] X.-L. Qi and S.-C. Zhang, *Reviews of Modern Physics* **83**, 1057 (2011).
- [2] M. Z. Hasan and C. L. Kane, *Reviews of Modern Physics* **82**, 3045 (2010).
- [3] P. Wei, F. Katmis, B. A. Assaf, H. Steinberg, P. Jarillo-Herrero, D. Heiman, and J. S. Moodera, *Physical Review Letters* **110**, 186807 (2013).
- [4] Y. Chen, J.-H. Chu, J. Analytis, Z. Liu, K. Igarashi, H.-H. Kuo, X. Qi, S.-K. Mo, R. Moore, D. Lu, *et al.*, *Science* **329**, 659 (2010).
- [5] M. Lang, M. Montazeri, M. C. Onbasli, X. Kou, Y. Fan, P. Upadhyaya, K. Yao, F. Liu, Y. Jiang, W. Jiang, *et al.*, *Nano Letters* **14**, 3459 (2014).
- [6] I. Vobornik, U. Manju, J. Fujii, F. Borgatti, P. Torelli, D. Krizmancic, Y. S. Hor, R. J. Cava, and G. Panaccione, *Nano letters* **11**, 4079 (2011).
- [7] A. Kandala, A. Richardella, D. W. Rench, D. M. Zhang, T. C. Flanagan, and N. Samarth, *Applied Physics Letters* **103**, 202409 (2013).
- [8] C.-Z. Chang, W. Zhao, D. Y. Kim, H. Zhang, B. A. Assaf, D. Heiman, S.-C. Zhang, C. Liu, M. H. W. Chan, and J. S. Moodera, *Nat Mater* **advance online publication** (2015).
- [9] C.-Z. Chang, J. Zhang, X. Feng, J. Shen, Z. Zhang, M. Guo, K. Li, Y. Ou, P. Wei, L.-L. Wang, *et al.*, *Science* **340**, 167 (2013).
- [10] S.-Y. Xu, M. Neupane, C. Liu, D. Zhang, A. Richardella, L. A. Wray, N. Alidoust, M. Leandersson, T. Balasubramanian, J. Sánchez-Barriga, *et al.*, *Nature Physics* **8**, 616 (2012).
- [11] Y. Hor, P. Roushan, H. Beidenkopf, J. Seo, D. Qu, J. Checkelsky, L. Wray, D. Hsieh, Y. Xia, S.-Y. Xu, *et al.*, *Physical Review B* **81**, 195203 (2010).
- [12] C.-Z. Chang, P. Tang, Y.-L. Wang, X. Feng, K. Li, Z. Zhang, Y. Wang, L.-L. Wang, X. Chen, C. Liu, *et al.*, *Physical Review Letters* **112**, 056801 (2014).
- [13] C.-Z. Chang, J. Zhang, M. Liu, Z. Zhang, X. Feng, K. Li, L.-L. Wang, X. Chen, X. Dai, Z. Fang, *et al.*, *Advanced Materials* **25**, 1065 (2013).
- [14] X.-L. Qi, T. L. Hughes, and S.-C. Zhang, *Physical Review B* **78**, 195424 (2008).
- [15] R. Yu, W. Zhang, H.-J. Zhang, S.-C. Zhang, X. Dai, and Z. Fang, *Science* **329**, 61 (2010).
- [16] C.-X. Liu, X.-L. Qi, X. Dai, Z. Fang, and S.-C. Zhang, *Physical Review Letters* **101**, 146802 (2008).
- [17] X. Kou, S.-T. Guo, Y. Fan, L. Pan, M. Lang, Y. Jiang, Q. Shao, T. Nie, K. Murata, J. Tang, *et al.*, *Physical review letters* **113**, 137201 (2014).
- [18] J. Checkelsky, R. Yoshimi, A. Tsukazaki, K. Takahashi, Y. Kozuka, J. Falson, M. Kawasaki, and Y. Tokura, *Nature Physics* **10**, 731–736 (2014).
- [19] C.-Z. Chang, P. Wei, and J. S. Moodera, *MRS Bulletin* **39**, 867 (2014).
- [20] M. Li, W. Cui, J. Yu, Z. Dai, Z. Wang, F. Katmis, W. Guo, and J. Moodera, *Phys. Rev. B* **91**, 014427 (2015).
- [21] V. Lauter, F. Katmis, B. Assaf, and J. Moodera, in *APS March Meeting Abstracts*, Vol. W (2014) p. 42.00007.
- [22] S. Ereemeev, V. Men'shov, V. Tugushev, P. M. Echenique, and E. V. Chulkov, *Physical Review B* **88**, 144430 (2013).
- [23] J. Kuneš and W. E. Pickett, *Physica B: Condensed Matter* **359**, 205 (2005).
- [24] L. Liu, *Solid State Communications* **46**, 83 (1983).
- [25] M. Franzblau, G. E. Everett, and A. Lawson, *Physical Review* **164**, 716 (1967).
- [26] S. Von Molnar and A. Lawson, *Physical Review* **139**, A1598 (1965).
- [27] W. Boncher, H. Dalafu, N. Rosa, and S. Stoll, *Coordination Chemistry Reviews* (2014).
- [28] V.-C. Lee and L. Liu, *Solid State Communications* **48**, 795 (1983).
- [29] M. Björck and G. Andersson, *Journal of Applied Crystallography* **40**, 1174 (2007).
- [30] A. Pimpinelli and J. Villain, *Physics of Crystal Growth* (Cambridge University Press, 1998) *Cambridge Books Online*.
- [31] M. Kiwi, *Journal of Magnetism and Magnetic Materials* **234**, 584 (2001).
- [32] R. Stamps, *Journal of Physics D: Applied Physics* **33**, R247 (2000).
- [33] J. Nogués and I. K. Schuller, *Journal of Magnetism and Magnetic Materials* **192**, 203 (1999).
- [34] R. Wen-Bin, H. Mao-Cheng, Y. Biao, S. Zhong, Z. Shi-Ming, X. Ming-Wen, G. Yuan, Z. Wei, S. Li, and D. Jun, *Chinese Physics B* **23**, 107502 (2014).
- [35] C. Schlenker, S. Parkin, J. Scott, and K. Howard, *Journal of magnetism and magnetic materials* **54**, 801 (1986).
- [36] R. Skomski, *Simple models of magnetism* (Oxford University Press Oxford, 2008).
- [37] N. Koon, *Physical review letters* **78**, 4865 (1997).
- [38] R. Skomski, O. Mryasov, J. Zhou, and D. J. Sellmyer, *Journal of applied physics* **99**, 08E916 (2006).
- [39] E. R. Callen and H. B. Callen, *Phys. Rev.* **129**, 578 (1963).
- [40] P. Bruno, *Journal of Physics F: Metal Physics* **18**, 1291

(1988).